

Relationship between the Corrosion Behavior and Oxide Property of HANA Alloys

Seung Jo Yoo*, Jeong-Yong Park, Byung-Kwon Choi and Yong Hwan Jeong
Advanced Core Materials Lab., Korea Atomic Energy Research Institute,
P.O Box 105 Yuseong, Deajeon 305-600, Korea
*ore78@naver.com

1. Introduction

HANA alloys were obtained an excellent corrosion resistance by means of optimizing the alloying elements and heat treatment process. The corrosion behavior of the HANA alloys was evaluated with the Zircaloy-4 as a reference alloy and the effect of the oxide properties on the corrosion behavior was also investigated. The corrosion testing was performed in the 360°C water and 360°C PWR-simulating loop conditions. The oxides formed on the HANA alloys were observed by an optical microscopy and a transmitted light optical microscopy to investigate their correlation with the regular transition behavior obtained in the corrosion data. We also examined the microstructure and second phase particles of the oxides of the HANA alloys and the reference alloy by using a transmission electron microscopy. From the ensemble of these observations, conclusions are derived about the relationship between the oxide properties and the corrosion behavior of the HANA alloys.

2. Experimental procedure

In this study, HANA-3, 6 and Zircaloy-4 alloys were used. The chemical composition of the HANA-3 and 6 alloys is Zr-1.5Nb-0.4Sn-0.1Fe-0.1Cu and Zr-1.1Nb-0.05Cu, respectively. The main difference between the Zircaloy-4 and HANA alloys is that the HANA alloys have Nb as a major alloying element but the Zircaloy-4 does not. From previous researches, Nb has been considered to be very effective for improving the corrosion resistance of the Zr-based alloys among the various alloying elements [1, 2].

Corrosion tests were performed in a 360°C water condition by using a static autoclave for 1020 days and in a 360°C PWR-simulation loop condition without a neutron flux for 1000 days (Temperature=360°C, Pressure=18.5~18.8MPa, Flow rate = 3~ 4 liter/h, pH 7, Li = 2.2 ppm, B = 650 ppm, O₂ < 5 ppb, H < 25 ppb) Corrosion testing specimens, 50 mm in length, were cut from the manufactured tubes and pickled in a solution of H₂O (30 vol.%), HNO₃ (30 vol.%), HCl (30vol.%) and HF (10vol.%). The corrosion resistance was evaluated by measuring the weight gain of the corroded samples after suspending the corrosion test at a periodic term. In order to understand how the oxide grows and how the microstructure evolves from the oxide/metal interface to the oxide/water surface, it is most profitable to use cross sectional samples. Therefore, in this study, only cross section samples were prepared and used for all the characterization techniques such as OM, TLOM and

TEM. The cross sectional samples which were prepared by a focused ion beam milling were used for the transmission electron microscopy.

3. Results and discussion

The corrosion kinetics of the Zircaloy-4 and HANA alloys was compared. Figure 1 shows the weight gain as a function of the exposure time collected from the corrosion test in the 360°C water and 360°C PWR-simulating loop conditions. In Figure 1, the corrosion rate of the HANA alloys was much lower than that of Zircaloy-4 and among the two types of HANA alloys, HANA-6 has the highest corrosion resistance in both conditions. An alloy showing a good corrosion resistance has less transition points during the corrosion test. Zircaloy-4 exhibited 6 transition points whereas HANA-6 showed just one transition point in the 360°C PWR-simulating loop condition.

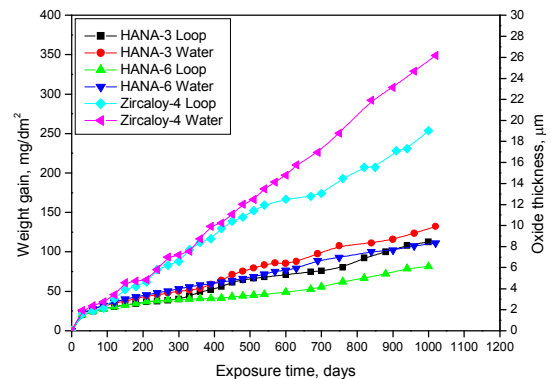


Figure 1. Corrosion behavior of HANA alloys and the Zircaloy-4 alloy in the 360°C water and 360°C PWR-simulating loop condition.

The general appearance of the cross sectional oxide layers was examined by an optical microscopy. From the observation of the cross sectional oxide samples, it was found that all the alloys have a uniform corrosion with no evidence of a localized corrosion and the roughness of the interface was almost the same in all alloys. And the measured oxide thicknesses were in good agreement with the oxide thickness converted from the weight gain data based on the relation that the weight gain of 15 mg/dm² = the oxide thickness of 1 μm.

The cross sectional oxide was also examined by using a transmitted light optical microscopy. When the thickness of the oxide sample reaches 5-8 μm, the sample becomes transparent to the visible light. In the case that the cross sectional oxides samples are

observed in the transmitted light mode, various light and dark bands parallel to the oxide/metal interface were observed. While the reflected light images show no contrast, periodic dark bands were observed in the transmitted light images for all the oxide layers.

The thicknesses of these bands were different depending on the alloy and corrosion condition. The observed thicknesses are approximately equal to the thickness of the oxides at the transition. In all the oxides, a black layer was formed at the oxide/metal interface. In the oxide formed on the Zircaloy-4 alloys in the 360 °C water condition, seven bands were counted whereas in the HANA-3 and 6 alloy oxides, 2 and 1 black bands were observed, respectively. The thickness of the layer was higher in the HANA alloys when compared to the Zircaloy-4 in both conditions. For instance, in the 360 °C water condition the HANA-6 alloy has the thickest oxide layer (5.7 μm) and the Zircaloy-4 has the thinnest oxide layer (2.4 μm). It implies that the thickness of the layer is larger in the alloys showing a better corrosion resistance.

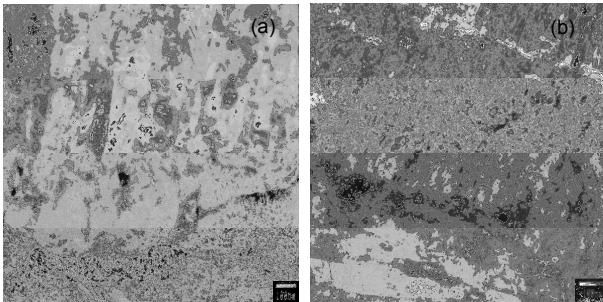


Figure 2. TEM microstructure of (a) the oxide/metal interface section of the oxide formed in the HANA-6 alloy and (b) the Zircaloy-4 in the 360 °C PWR-simulating loop condition.

Focused ion beam milled cross sectional samples were examined by using a transmission electron microscopy. In the oxides, both columnar and small equiaxed grains were observed in all the alloys. However, the grain size of the oxide was different depending on the alloy and corrosion condition. HANA alloys had larger columnar and equiaxed grains than the Zircaloy-4.

The morphologies of the oxide and incorporated precipitates are shown in Figures 2 and 3. Figure 2 shows that the columnar oxide grains grow in the direction perpendicular to the oxide/metal interface and cracks were observed in the oxide layers. The oxide around the cracks exhibits more equiaxed grains than in the bulk of the oxide. In figure 2 (b), the oxide of the Zircaloy-4, a grain decohesion was observed between the small equiaxed and narrow-short columnar grains.

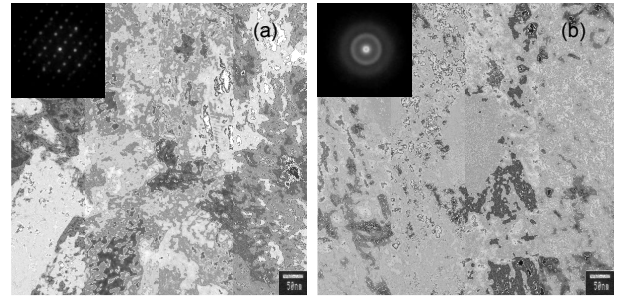


Figure 3. TEM microstructure of (a) a metallic and (b) amorphous precipitate incorporated in the oxide formed on the HANA-3 alloy in the 360 °C water condition.

Second phase particles were incorporated as unoxidized ones into the oxide layer. The metallic second phase particles were observed in the oxide near the oxide/metal interface. After a certain distance from the oxide/metal interface into the oxide layer, both amorphous and oxidized second phase particles were found as shown in Figure 3 (b). Based on the results obtained in this study, the oxides of the HANA alloys have a more protective nature against an oxygen diffusion when compared to the Zircaloy-4.

4. Conclusion

The HANA alloys showed a better corrosion resistance than the Zircaloy-4 based on the corrosion tests in the 360 °C water and 360 °C PWR-simulating loop conditions. The oxides formed on the HANA-3, 6 and Zircaloy-4 alloys were investigated by various techniques such as OM, TLOM, and TEM. The oxide properties revealed that the oxides of the HANA alloys have a more protective nature against an oxygen diffusion when compared to the Zircaloy-4 alloy.

Acknowledgements

This study was supported by KOSEF and MOST, Korean government, through its National Nuclear Technology Program.

REFERENCES

- [1] A.V. Nikulina, J. Nucl. Mater. 238 (1996) 205.
- [2] R.J. Comstock, G. Schoenberger, G.P. Sabol, ASTM STP 1295 (1996) 710.